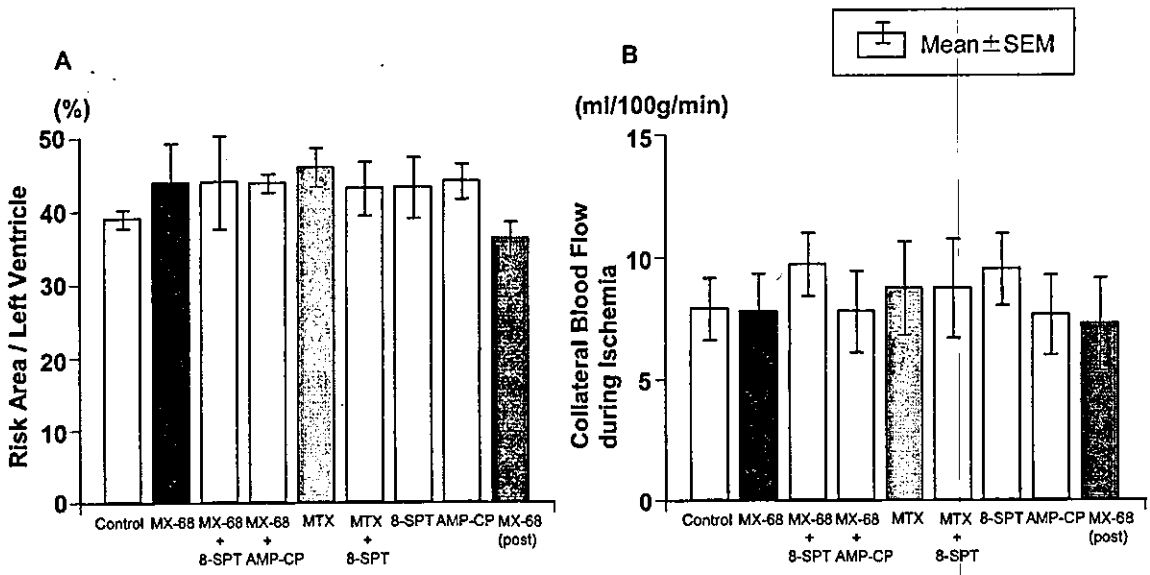

FIGURE 2. Area at risk (A) and collateral blood flow during ischemia (B) in the control group, MTX group, MX-68 group, MTX+8-SPT group, MX-68+8-SPT group, MX-68+AMP-CP group, MX-68(post) group, 8-SPT group, and AMP-CP group. There were no differences of the area at risk and collateral flow during ischemia between these groups. Statistical significance was tested by ANOVA.

blunted by infusion of either 8-SPT or AMP-CP. MTX also reduced infarct size in a similar manner to MX-68, and its protective effect was blunted by 8-SPT. Even when MX-68 was administered after the start of reperfusion, reduction of infarct size was observed to a level between that in the control group and that when MX-68 was administered before ischemia. Regression plots of infarct size versus collateral blood flow are shown in Figure 4, which indicate that the infarct size-limiting effect of either MX-68 or MTX was attributable to an adenosine-dependent mechanism.

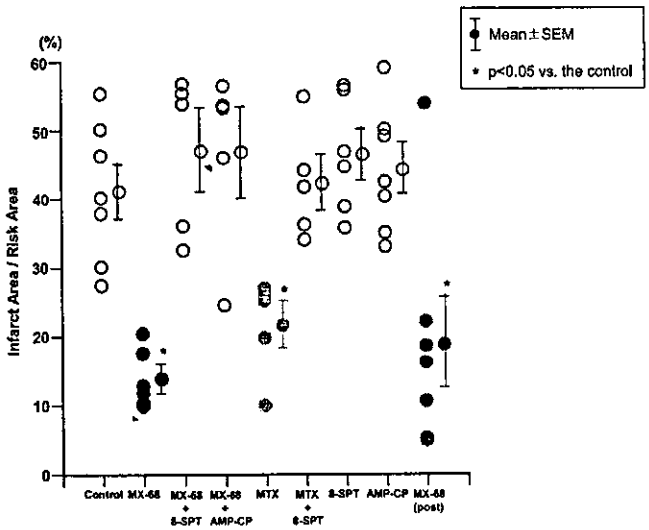

FIGURE 3. Infarct size expressed as a percentage of the area at risk. Infarct size was markedly decreased in the MTX and MX-68 groups compared with the control group, and this improvement was completely reversed by 8-SPT or AMP-CP. Statistical significance was tested by ANOVA.

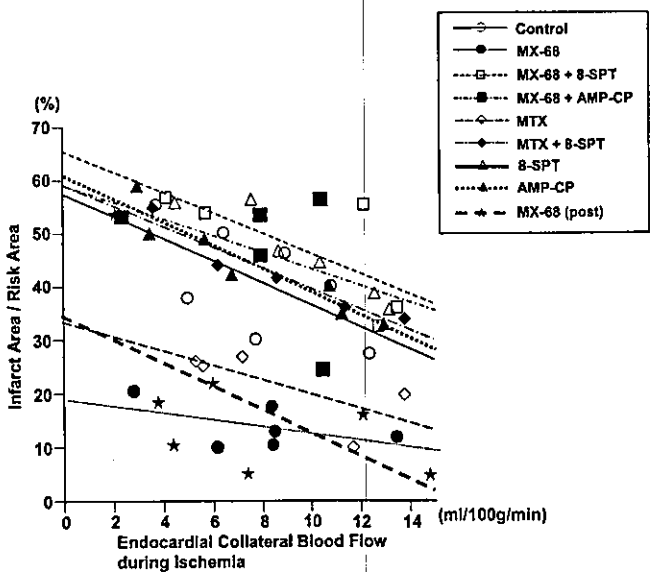

FIGURE 4. Infarct size after 90 minutes of ischemia versus regional collateral flow during ischemia. Infarct size is expressed as a percentage of the area at risk. Infarct size was markedly decreased in the MTX and MX-68 groups compared with the control group. This improvement was completely reversed by 8-SPT or AMP-CP. Statistical significance was tested by ANCOVA.

DISCUSSION

The present study demonstrated that either MTX or MX-68 could markedly reduce infarct size and that the cardioprotective effects of these agents were attributable to ecto-5′-nucleotidase- and adenosine-dependent mechanisms.

Adenosine and the Cardioprotective Effect of MTX or MX-68

Anti-inflammatory drugs such as steroids were thought to have an infarct size-limiting effect[7,8] because the pathophysiology of myocardial infarction resembles tissue inflammation and such drugs can potently ameliorate the tissue inflammatory process. However, steroids and related hormones have been variously reported to decrease infarct size, have no effect, or even increase infarct size.[4,9] On the other hand, other anti-inflammatory agents seem to be effective against ischemia/reperfusion injury. For example, 17β-estradiol is known to have an anti-inflammatory effect[10] and it markedly reduces infarct size.[11] Statins are known to improve vascular inflammation and atherosclerosis, and these drugs also reduce infarct size markedly.[12] Therefore, we cannot necessarily conclude that all anti-inflammatory drugs will be effective for ischemia/reperfusion injury, but we can suggest that these drugs have the possibility of mediating cardioprotection.

MTX and its analog MX-68 are disease-modifying antirheumatic drugs,[20] and their mechanism of action on immune cells was recently reported to be mediated via adenosine.[13] If this is the case in myocardial cells, either MTX or MX-68 would limit infarct size because adenosine markedly reduces the size of infarcts and triggers/mediates the cardioprotective effect of ischemic preconditioning.[24,25] Indeed, the present study revealed that MTX and its analog (MX-68) can ameliorate ischemia/reperfusion injury. We also showed that this action is adenosine-dependent, because the effect of either MTX or MX-68 was blunted by 8-SPT, an adenosine receptor antagonist. Accordingly, both MTX and MX-68 ameliorate ischemia/reperfusion injury via adenosine-related mechanisms.

In immune system cells, the adenosine-related action of MTX was reported to be attributable to ecto-5′-nucleotidase,[13] and this also seems to be the case in the myocardium because the effect of MX-68 and MTX was blunted by an ecto-5′-nucleotidase inhibitor or an adenosine receptor antagonist. Ecto-5′-nucleotidase produces adenosine, and adenosine inhibits norepinephrine release from presynaptic vesicles and attenuates Ca^{2+} influx into myocytes by acting on A_1 receptors and inhibitory G protein.[26,27] Adenosine also increases CBF, inhibits platelet aggregation, and inhibits leukocyte activation via A_2 receptors and stimulatory G protein.[14,16] Since factors such as an increase of norepinephrine, Ca^{2+} overload, decreased CBF, and activation of platelets and leukocytes are deleterious to the heart, control of these factors by adenosine may help to minimize ischemia/reperfusion injury. Several studies have shown that adenosine administration markedly attenuates ischemia/reperfusion injury.[3,15,17]

Role of Adenosine in the Effect of MTX or MX-68

How does MTX or MX-68 act on ecto-5′-nucleotidase? Several possibilities can be suggested. First, activation of ecto-5′-nucleotidase may occur after phosphorylation, as seen with ischemic preconditioning or treatment with phorbol ester, where activation of protein kinase C possibly leads to the phosphorylation and activation of ecto-5′-nucleotidase.[28,29] However, the in vitro activity of myocardial ecto-5′-nucleotidase was not increased by brief exposure to MTX (data not shown), whereas methoxamine and phorbol ester, which phosphorylate and activate ecto-5′-nucleotidase, both activated myocardial ecto-5′-nucleotidase in vitro.[28,29] These results suggest that MTX does not activate ecto-5′-nucleotidase via the process of phosphorylation, so a direct interaction between MTX and the active site of ecto-5′- nucleotidase may be responsible instead.

Second, MTX is reported to increase the tissue level of AICA riboside by inhibition of AICA riboside deaminase,[13] and we have previously shown that AICA riboside increases the activity of ecto-5′-nucleotidase.[19] Therefore, ecto-5′-nucleotidase may be activated when the myocardial AICA riboside is increased during administration of MTX in vivo. However, it has not been clarified how AICA riboside activates ecto-5′-nucleotidase in the heart. Since AICA riboside activates AMP deaminase and inactivates adenosine deaminase, it may also modulate the enzymes related to adenosine metabolism.[30] Accordingly, AICA riboside could increase adenosine production via activation of ecto-5′-nucleotidase, and maintain a high adenosine level by inhibiting enzymes involved in the metabolism of adenosine. In this context, there are many reports that AICA riboside is cardioprotective against ischemia/reperfusion injury via adenosine-dependent mechanisms.[16,30,31]

Clinical Relevance and Limitations

In this study, we demonstrated that both MX-68 and MTX can limit infarct size via adenosine-dependent mechanisms. It would be of interest to test the cardioprotective effect of MTX or MX-68 in the clinical setting of acute myocardial infarction with coronary revascularization, since infusion of adenosine during reperfusion has been shown to limit infarct size.[17] Furthermore, since administration of adenosine can precondition the myocardium prior to sustained ischemia,[24] treatment with MTX or MX-68 may be useful in patients who have coronary artery disease to precondition the myocardium and improve resistance to acute myocardial infarction. However, further studies are necessary to develop either MTX or MX-68 as a drug to treat acute ischemic heart disease.

REFERENCES

1. Resnekov L. The intermediate coronary care unit. A stage in continued coronary care. *Br Heart J.* 1977;39:357–362.
2. Geltman EM, Ehsani AA, Campbell MK, et al. The influence of location and extent of myocardial infarction on long-term ventricular dysrhythmia and mortality. *Circulation.* 1979;60:805–814.
3. Kitakaze M, Hori M. It is time to ask what adenosine can do for cardioprotection (Brief Review). *Heart Vessels.* 1998;13:211–228.
4. Scheuer DA, Mifflin SW. Chronic corticosterone treatment increases myocardial infarct size in rats with ischemia-reperfusion injury. *Am J Physiol.* 1997;272:R2017–R2024.
5. Chapman DW, Skaggs RH, Thomas JR, et al. The effect of cortisone in experimental myocardial infarction. *Am J Med Sci.* 1952;223:41–44.
6. Roberts R, Demello V, Sobel BE. Deleterious effects of methylprednisolone in patients with myocardial infarction. *Circulation.* 1976;53(Suppl I):I204–I206.
7. Braunwald E, Maroko PR. Effects of hyaluronidase and hydrocortisone on myocardial necrosis after coronary occlusion. *Am J Cardiol.* 1976;37:550–556.
8. Shatney CH, MacCarter DJ, Lillehei RC. Temporal factors in the reduction of myocardial infarct volume by methylprednisolone. *Surgery.* 1976;80:61–69.
9. Madias JE, Hood WB Jr. Effects of methylprednisolone on the ischemic damage in patients with acute myocardial infarction. *Circulation.* 1982;65:1106–1113.
10. Squadrito F, Altavilla D, Squadrito G, et al. 17Beta-oestradiol reduces cardiac leukocyte accumulation in myocardial ischaemia reperfusion injury in rat. *Eur J Pharmacol.* 1997;335:185–192.
11. Hale SL, Birnbaum Y, Kloner RA. Beta-Estradiol, but not alpha-estradiol, reduced myocardial necrosis in rabbits after ischemia and reperfusion. *Am Heart J.* 1996;132:258–262.
12. Scalia R, Gooszen ME, Jones SP, et al. Simvastatin exerts both anti-inflammatory and cardioprotective effects in apolipoprotein E-deficient mice. *Circulation.* 2001;103:2598–2603.
13. Babbitt TG, Virmani R, Norton R Jr, et al. Adenosine administration during reperfusion following 3 hours of ischemia: Effects on infarct size, ventricular function, and regional myocardial blood flow. *Am Heart J.* 1990;120:808–818.
14. Dorheim TA, Hoffman A, Van Wylen DGL, et al. Enhanced interstitial fluid adenosine attenuates myocardial stunning. *Surgery.* 1991;110:136–145.
15. Morabito L, Montesinos MC, Schreibman DM, et al. Methotrexate and sulfasalazine promote adenosine release by a mechanism that requires ecto-5′-nucleotidase-mediated conversion of adenine nucleotides. *J Clin Invest.* 1998;101:295–300.
16. Cronstein BN, Levin RI, Belanoff J, et al. Adenosine: an endogenous inhibitor of neutrophil-mediated injury to endothelial cells. *J Clin Invest.* 1986;78:760–770.
17. Kitakaze M, Hori M, Kamada T. The role of adenosine and its interaction with alpha-adrenoceptor activity in myocardial ischemic and reperfusion injury (Brief Review). *Cardiovasc Res.* 1993;27:18–27.
18. Kitakaze M, Minamino T, Node K, et al. Adenosine and cardioprotection in the diseased heart (Brief Review). *Jpn Circ J.* 1999;63:231–243.
19. Hori M, Kitakaze M, Takashima S, et al. AICA riboside improves myocardial ischemia in coronary microembolization in dogs. *Am J Physiol.* 1994;267:H1483–H1495.
20. Mihara M, Urakawa K, Takagi N, et al. In vitro and in vivo biological activities of a novel nonpolyglutamable anti-folate, MX-68. *Immunopharmacology.* 1996;35:41–46.
21. Kitakaze M, Hori M, Morioka T, et al. Alpha$_1$-adrenoceptor activation mediates the infarct size limiting effect of ischemic preconditioning through augmentation of 5′-nucleotidase activity and adenosine release. *J Clin Invest.* 1994;93:2197–2205.
22. Winer BJ. *Statistical Principles in Experimental Design.*2nd ed. New York: McGraw-Hill, Inc.; 1982:1–907.
23. Snedecor GW, Cochran WG. *Statistical Methods.* 6th ed. Ames, Iowa: Iowa State University Press; 1972:258–298.
24. Liu GS, Thornton J, Van Winkle DM, et al. Protection against infarction afforded by preconditioning is mediated by A1 adenosine receptors in rabbit heart. *Circulation.* 1991;84:350–356.
25. Kitakaze M, Hori M, Takashima S, et al. Ischemic preconditioning increases adenosine release and 5′-nucleotidase activity during myocardial ischemia and reperfusion in dogs: Implication for myocardial salvage. *Circulation.* 1993;87:208–215.
26. Richardt G, Wassa W, Kranzhofer R, et al. Adenosine inhibits exocytotic release of endogenous noradrenaline in rat heart: A protective mechanisms in early myocardial ischemia. *Circ Res.* 1987;61:117–123.
27. Sato H, Hori M, Kitakaze M, et al. Endogenous adenosine blunts β-adrenoceptor-mediated inotropic response in hypoperfused canine myocardium. *Circulation.* 1992;85:1594–1603.
28. Kitakaze M, Node K, Minamino T, et al. Role of activation of protein kinase C in the infarct size-limiting effect of ischemic preconditioning through activation of ecto-5′-nucleotidase. *Circulation.* 1996;93:781–791.
29. Kitakaze M, Minamino T, Node K, et al. Activation of ecto-5′-nucleotidase by protein kinase C attenuates irreversible cellular injury due to hypoxia and reoxygenation in rat cardiomyocytes. *J Mol Cell Cardiol.* 1996;28:1945–1955.
30. Gruber HE, Hoffer ME, McAllister DR, et al. Increased adenosine concentration in blood from ischemic myocardium by AICA riboside. Effects on flow, granulocyte, and injury. *Circulation.* 1989;80:1400–1411.
31. Kitakaze M, Takashima S, Minamino T, et al. Improvement by 5-amino-4-imidazole carboxamide riboside of the contractile dysfunction that follows brief periods of ischemia through increases in ecto-5-nucleotidase activity and adenosine release in canine hearts. *Jpn Circ J.* 1999;63:542–553.

Japanese Journal of Applied Physics
Vol. 43, No. 10, 2004, pp. 7324–7328

Quasi-Monochromatic Flash X-Ray Generator Utilizing Disk-Cathode Molybdenum Tube

Eiichi SATO, Michiaki SAGAE, Etsuro TANAKA[1], Yasuomi HAYASI, Rudolf GERMER[2], Hidezo MORI[3], Toshiaki KAWAI[4], Toshio ICHIMARU[5], Shigehiro SATO[6], Kazuyoshi TAKAYAMA[7] and Hideaki IDO[8]

Department of Physics, Iwate Medical University, 3-16-1 Honchodori, Morioka 020-0015, Japan
[1]*Department of Nutritional Science, Faculty of Applied Bio-science, Tokyo University of Agriculture, 1-1-1 Sakuragaoka, Setagaya-ku 156-8502, Japan*
[2]*ITP, FHTW FB1 and TU-Berlin, Blankenhainer Str. 9, D 12249 Berlin, Germany*
[3]*Department of Cardiac Physiology, National Cardiovascular Center Research Institute, 5-7-1 Fujishiro-dai, Suita, Osaka 565-8565, Japan*
[4]*Electron Tube Division #2, Hamamatsu Photonics Inc., 314-5 Shimokanzo, Toyooka Village, Iwata-gun 438-0193, Japan*
[5]*Department of Radiological Technology, School of Health Sciences, Hirosaki University, 66-1 Honcho, Hirosaki 036-8564, Japan*
[6]*Department of Microbiology, School of Medicine, Iwate Medical University, 19-1 Uchimaru, Morioka 020-8505, Japan*
[7]*Shock Wave Research Center, Institute of Fluid Science, Tohoku University, 2-1-1 Katahira, Aoba-ku, Sendai 980-8577, Japan*
[8]*Department of Applied Physics and Informatics, Faculty of Engineering, Tohoku Gakuin University, 1-13-1 Chuo, Tagajo 985-8537, Japan*

(Received April 2, 2004; accepted June 14, 2004; published October 8, 2004)

High-voltage condensers in a polarity-inversion two-stage Marx surge generator are charged from −40 to −60 kV using a power supply, and the electric charges in the condensers are discharged to an X-ray tube after closing the gap switches in the surge generator using a trigger device. The X-ray tube is a demountable diode, and the turbomolecular pump evacuates air from the tube with a pressure of approximately 1 mPa. Sharp K-series characteristic X-rays of molybdenum are produced without using a monochromatic filter, since the tube utilizes a disk cathode and a rod target, and bremsstrahlung rays are not emitted in the opposite direction to that of electron acceleration. The peak tube voltage increased with increasing charging voltage and increasing space between the target and cathode electrodes. At a charging voltage of −60 kV and a target-cathode space of 1.0 mm, the peak tube voltage and current were 110 kV and 0.75 kA, respectively. The pulse width ranged from 40 to 100 ns, and the maximum dimension of the X-ray source was 3.0 mm in diameter. The number of generator-produced K photons was approximately 7×10^{14} photons/cm^2·s at 0.5 m from the source. [DOI: 10.1143/JJAP.43.7324]

KEYWORDS: flash X-ray, characteristic X-ray, quasi-monochromatic radiography, bremsstrahlung X-ray distribution

1. Introduction

Flash X-ray generators have been developed as a powerful tool in high-speed radiography because they produce extremely short X-ray pulses of less than 1 μs. Currently, most generators utilize a multistage Marx surge generator[1,2] in order to produce high-photon-energy flash X-rays by increasing the maximum tube voltage. On the other hand, soft flash X-ray generators[3–7] with photon energies of less than 150 keV can be applied to biomedicine, and the repetition rate has been increased to the sub-kilohertz order.[8]

High-dose-rate monochromatic X-rays are produced by a synchrotron in conjunction with single crystals and have been applied to X-ray phase imaging[9,10] and microangiography.[11] Subsequently, because extremely high-dose-rate quasi-monochromatic X-rays are produced from the axial direction of weakly ionized linear plasma,[12–14] high-speed biomedical radiography has been performed. However, the bremsstrahlung X-rays are produced using targets of molybdenum, silver, cerium, and tungsten, since high-photon-energy bremsstrahlung X-rays are not absorbed effectively in the linear plasma. In addition, in cases where cold cathode triodes are employed, it is difficult to increase the condenser charging voltage to increase the photon energies of characteristic X-rays due to vacuum breakdown; the target voltage is equal to the charging voltage.

Because bremsstrahlung X-ray intensity varies with changes in the angle and direction of electron acceleration, characteristic X-rays are produced without using a monochromatic filter by selecting the irradiation direction. Although bremsstrahlung intensity is proportional to the atomic number, the angle selection will be a useful technique to produce quasi-monochromatic X-rays.

In this article, we describe a compact flash X-ray generator utilizing a molybdenum-target radiation tube, used to perform a preliminary experiment for generating quasi-monochromatic X-rays using the angle dependence of bremsstrahlung rays.

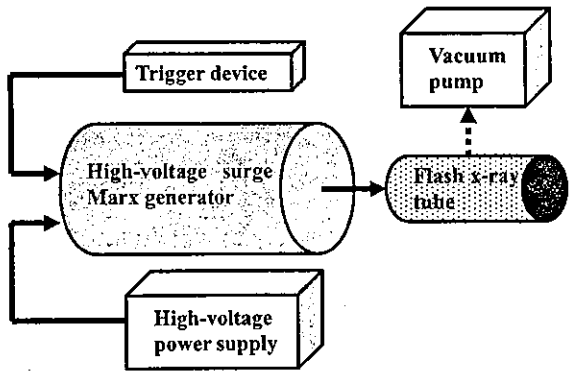

Fig. 1. Block diagram of compact quasi-monochromatic flash X-ray generator.

2. Generator

2.1 *High-voltage circuit*

Figure 1 shows a block diagram of a compact quasi-monochromatic flash X-ray generator. This generator consists of the following components: a constant high-voltage power supply, a polarity-inversion two-stage surge Marx generator with a capacity during main discharge of 425 pF, a trigger device for the surge generator, a turbomolecular pump, and a flash X-ray tube. Since the electric circuit of the surge generator employs a polarity-inversion two-stage Marx line (Fig. 2), the surge produces twice the potential of the condenser charging voltage. When two condensers inside of the surge generator are charged from −40 to

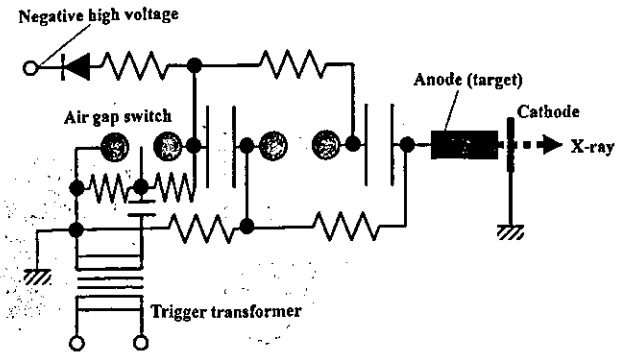

Fig. 2. Circuit diagram of flash X-ray generator.

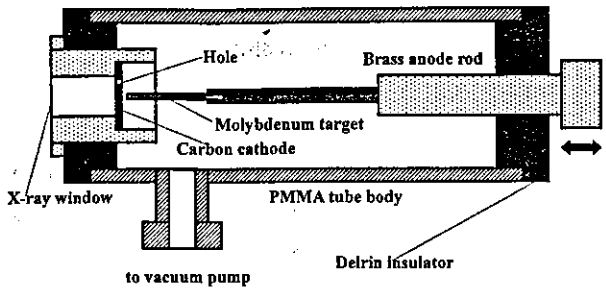

Fig. 3. Schematic drawing of flash X-ray tube.

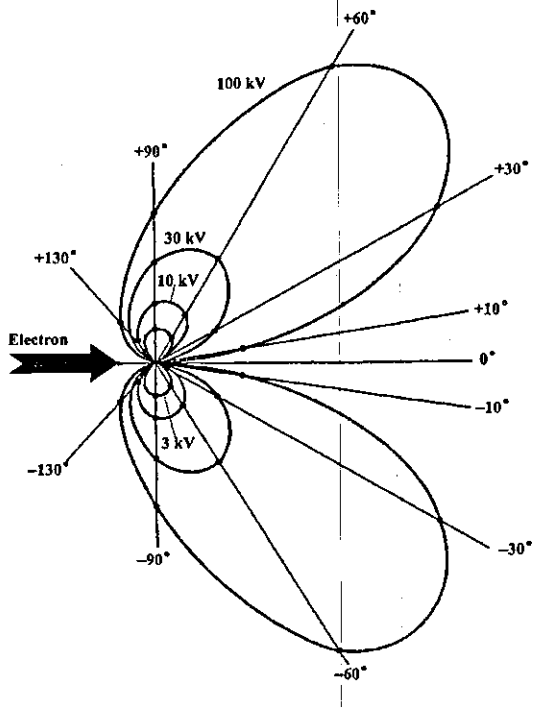

Fig. 4. Bremsstrahlung X-ray intensity distribution vs angle.

−60 kV, the ideal output voltage ranges from 80 to 120 kV.

2.2 *X-ray tube*

The X-ray tube is of the demountable diode type, as illustrated in Fig. 3. This tube is connected to the turbomolecular pump with a pressure of approximately 1 mPa and consists of the following major devices: a rod-shaped molybdenum target, a disk cathode made of graphite, a polyethylene terephthalate (Mylar) X-ray window 0.25 mm in thickness, and a polymethyl methacrylate (PMMA) tube body. The target-cathode (T–C) space was regulated from the outside of the X-ray tube by rotating the anode rod, and the transmission X-rays are obtained through a 1.0 mm-thick graphite cathode and an X-ray window. Because bremsstrahlung rays are not emitted in the opposite direction to that of electron acceleration (Fig. 4), characteristic X-rays can be produced.

3. Characteristics

3.1 *Tube voltage and current*

Tube voltage and current were measured using a high-voltage divider with an input impedance of 10 kΩ and a current transformer, respectively (Figs. 5 and 6). The voltage and current roughly displayed damped oscillations. At a constant T–C space of 1.0 mm, peak voltage increased slightly with increasing charging voltage. In contrast, peak

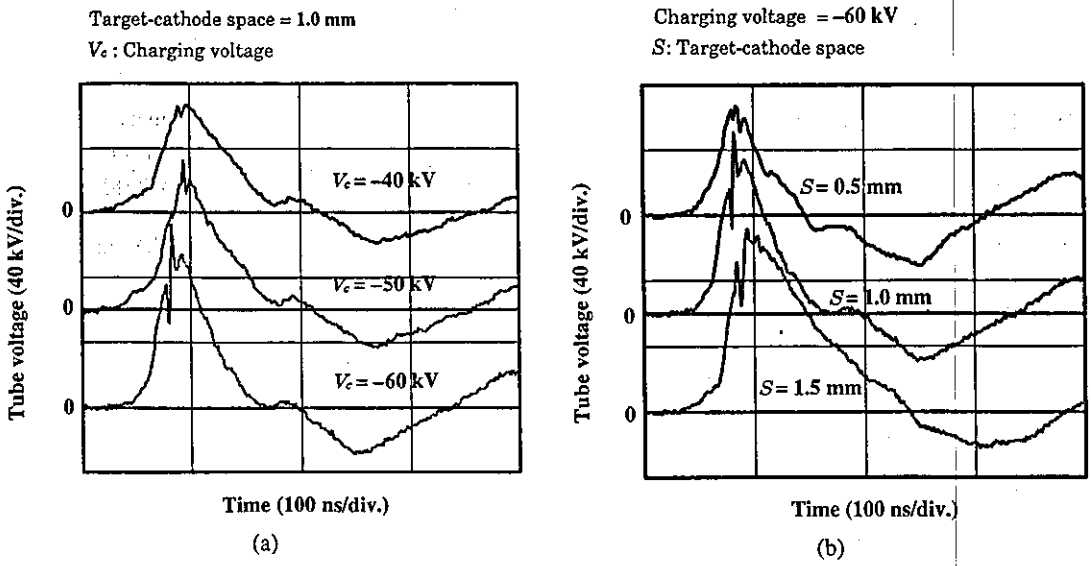

Fig. 5. Variations in tube voltage with changes in (a) charging voltage and (b) space.

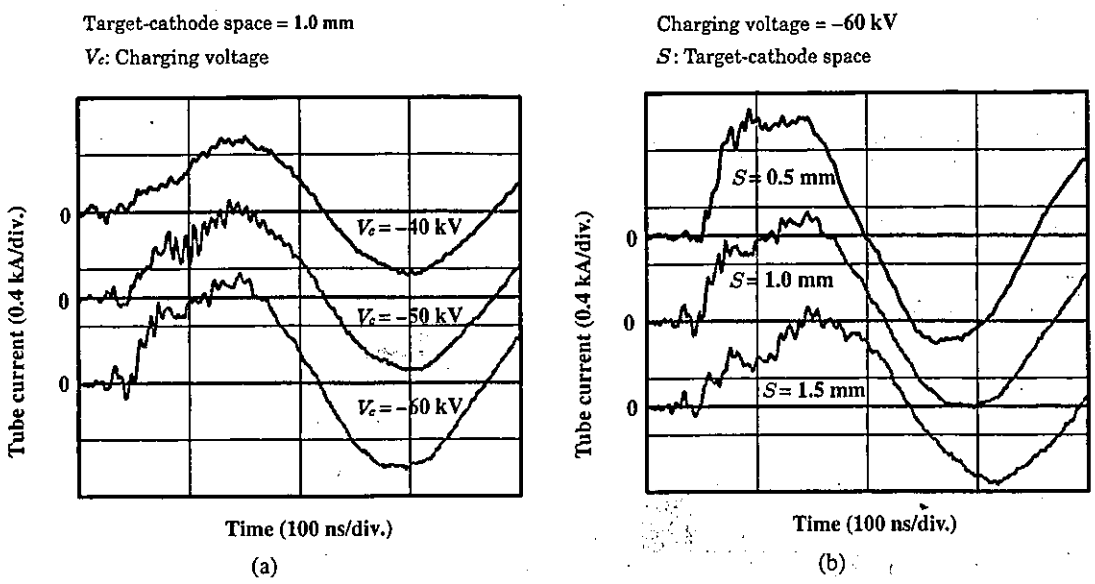

Fig. 6. Tube currents with changes in (a) charging voltage and (b) space.

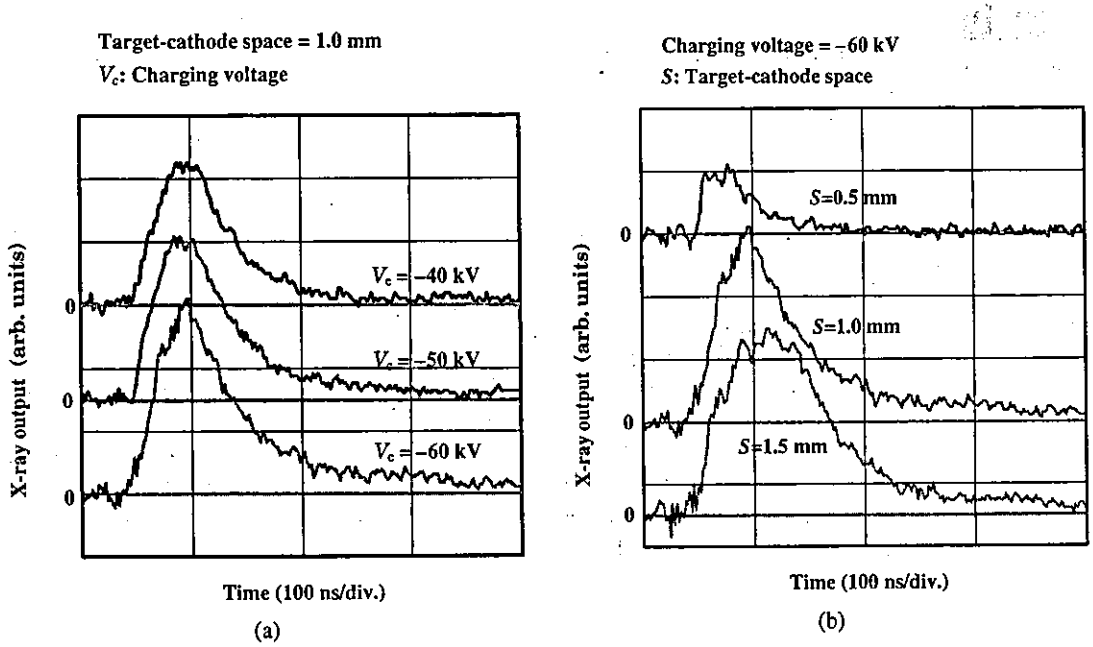

Fig. 7. X-ray outputs according to changes in (a) charging voltage and (b) space.

voltage substantially increased when T–C space was increased at a constant charging voltage of −60 kV. Subsequently, peak tube current increased with increasing charging voltage. When T–C space was increased, current rise time increased, and peak current decreased. At a charging voltage of −60 kV and a T–C space of 1.0 mm, peak tube voltage and current were 110 kV and 0.75 kA, respectively.

3.2 *X-ray output*

X-ray output pulse was detected using a combination of a plastic scintillator and a photomultiplier (Fig. 7). When the charging voltage was increased, the pulse height increased, but the width seldom varied. Next, with increases in the T–C space, the height was maximized, and the width increased. In the present work, the width ranged from 40 to 100 ns. Next, the time-integrated X-ray intensity measured using a thermoluminescence dosimeter (Kyokko TLD Reader 1500 having MSO-S elements without energy compensation) was approximately 3.0 μC/kg at 0.5 m from the X-ray source with a charging voltage of −60 kV and a T–C space of 1.0 mm.

3.3 *X-ray source*

In order to measure the images of the X-ray source, we employed a pinhole camera with a hole diameter of 100 μm (Fig. 8). When the charging voltage was increased, the plasma X-ray source grew, and both spot dimension and intensity increased. The maximum dimension was almost equal to the target diameter and had a value of approximately 3.0 mm.

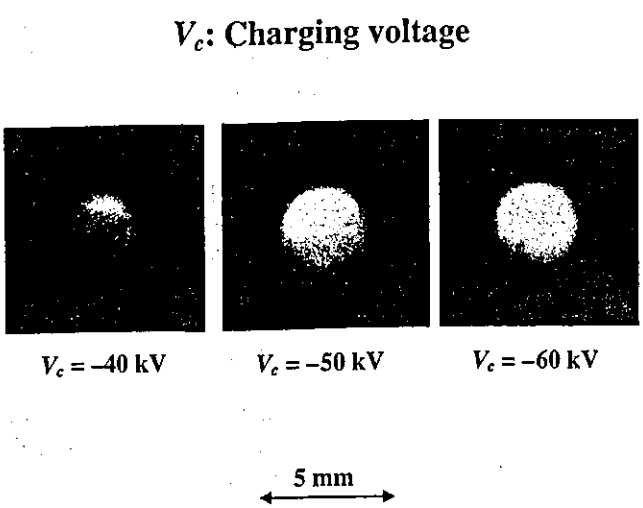

Fig. 8. Images of X-ray source with changes in charging voltage at constant space between target and cathode electrodes.

3.4 X-ray spectra

X-ray spectra were measured by a transmission-type spectrometer with a lithium fluoride curved crystal 0.5 mm in thickness. The spectra were measured using a computed radiography (CR) system[15] (Konica Regius 150) with a wide dynamic range, and relative X-ray intensity was calculated from Dicom digital data. Figure 9 shows the measured spectra from the molybdenum target. We observed sharp lines of K-series characteristic X-rays, while bremsstrahlung rays were hardly detected. The characteristic X-ray intensity of the Kα and Kβ lines substantially increased with increasing charging voltage.

4. Radiography

Flash radiography was performed using the CR system at 0.5 m from the X-ray source, and the charging voltage and the T–C space were −60 kV and 1.0 mm, respectively.

Firstly, rough measurements of spatial resolution were made using wires. Figure 10 shows radiograms of tungsten wires coiled around a pipe made of polymethyl methacrylate. Although the image contrast increased with increasing wire diameter, a 50-μm-diameter wire could be observed.

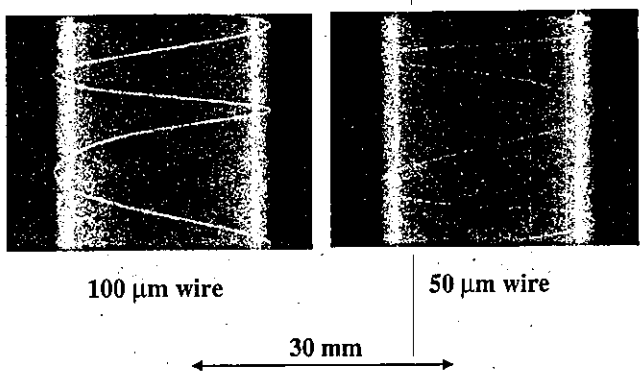

Fig. 10. Radiograms of tungsten wires of 50 and 100 μm in diameter coiled around pipes made of polymethyl methacrylate.

An image of plastic bullets falling into a polypropylene beaker from a glass test tube is shown in Fig. 11. Because the X-ray pulse widths were approximately 60 ns, the stop-motion image of bullets could be obtained. Figure 12 shows an angiogram of a rabbit heart; iodine-based microspheres of 15 μm in diameter were used, and fine blood vessels of approximately 100 μm were visible.

5. Discussion

Concerning the spectrum measurement, sharp molybdenum K-series characteristic X-rays were obtained, and monochromatic Kα lines can be obtained using a zirconium filter. The photon energies of characteristic X-rays are determined by the target element, and the X-ray intensity increases with increasing tube voltage by increasing the charging voltage. As compared with the plasma flash X-ray generator utilizing a molybdenum target triode,[13] bremsstrahlung X-rays were hardly observed at all even when higher tube voltages were applied to the diode, since the characteristic X-rays were produced from the target tip. Because the maximum tube voltage can be increased easily, and high-photon-energy K-series characteristic X-rays from

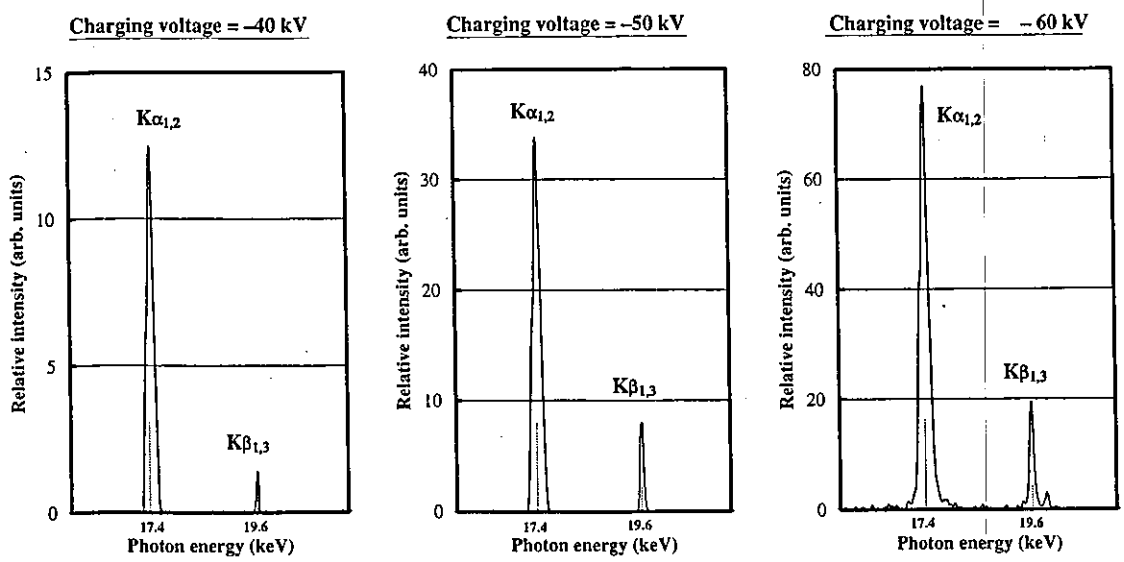

Fig. 9. X-ray spectra from weakly ionized molybdenum plasma according to changes in charging voltage with space of 1.0 mm.

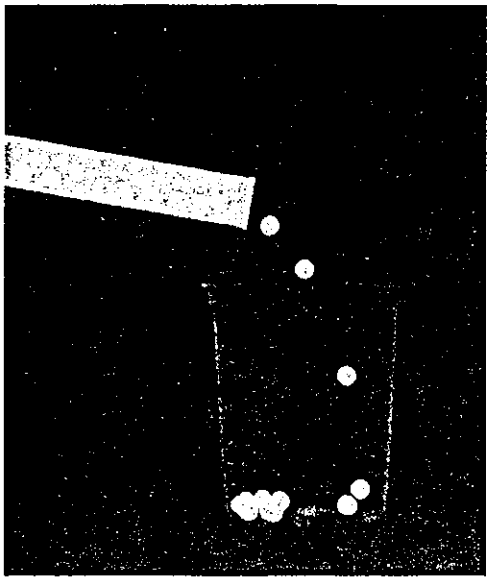

Fig. 11. Radiograms of plastic bullets falling into polypropylene beaker from glass test tube.

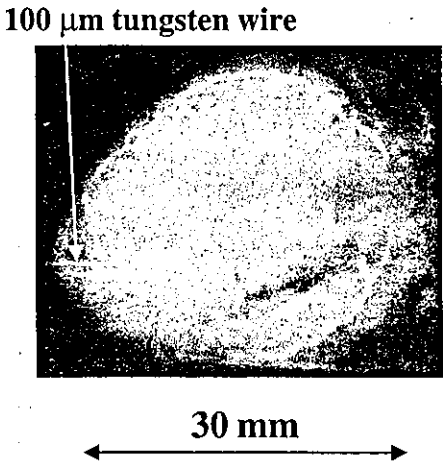

Fig. 12. Angiogram of rabbit heart.

the cerium or tungsten target can be produced. In particular, the cerium target is very useful in order to perform microangiography using iodine-based contrast mediums.

In this research, although the number of generator-produced characteristic K photons was approximately 7×10^{14} photons/cm^2·s at 0.5 m from the source, the number can be increased easily by increasing the electrostatic energy in the condensers.

Using this generator, because the photon energies of characteristic X-rays can be selected, various quasi-monochromatic high-speed radiographies, such as high contrast microangiography and photon-counting radiography for decreasing noise from radiograms, will be possible.

Acknowledgment

This work was supported by Grants-in-Aid for Scientific Research (13470154, 13877114, and 16591222) and Advanced Medical Scientific Research from MECSST, Grants from Keiryo Research Foundation, JST (Test of Fostering Potential), NEDO, and MHLW (HLSRG, RAMT-nano-001, RHGTEFB-genome-005, and RGCD13C-1).

1) A. Mattsson: Physica Scripta **5** (1972) 99.
2) R. Germer: J. Phys. E: Sci. Instrum. **12** (1979) 336.
3) E. Sato, H. Isobe and F. Hoshino: Rev. Sci. Instrum. **57** (1986) 1399.
4) E. Sato, M. Sagae, K. Takahashi, A. Shikoda, T. Oizumi, Y. Hayasi, Y. Tamakawa and T. Yanagisawa: Med. & Biol. Eng. & Comput. **32** (1994) 295.
5) A. Shikoda, E. Sato, M. Sagae, T. Oizumi, Y. Tamakawa and T. Yanagisawa: Rev. Sci. Instrum. **65** (1994) 850.
6) E. Sato, M. Sagae, A. Shikoda, K. Takahashi, T. Oizumi, M. Yamamoto, A. Takabe, K. Sakamaki, Y. Hayasi, H. Ojima, K. Takayama and Y. Tamakawa: Proc. SPIE **2869** (1996) 937.
7) K. Takahashi, E. Sato, M. Sagae, T. Oizumi, Y. Tamakawa and T. Yanagisawa: Jpn. J. Appl. Phys. **33** (1994) 4146.
8) E. Sato, K. Takahashi, M. Sagae, S. Kimura, T. Oizumi, Y. Hayasi, Y. Tamakawa and T. Yanagisawa: Med. & Biol. Eng. & Comput. **32** (1994) 289.
9) T. J. Davis, D. Gao, T. E. Gureyev, A. W. Stevenson and S. W. Wilkins: Nature **373** (1995) 595.
10) A. Momose, T. Takeda, Y. Itai and K. Hirano: Nature Medicine **2** (1996) 473.
11) H. Mori *et al.*: Radiology **201** (1996) 173.
12) E. Sato, Y. Hayasi, R. Germer, E. Tanaka, H. Mori, T. Kawai, H. Obara, T. Ichimaru, K. Takayama and H. Ido: Jpn. J. Med. Imag. Inform. Sci. **20** (2003) 148.
13) E. Sato, Y. Hayasi, R. Germer, E. Tanaka, H. Mori, T. Kawai, H. Obara, T. Ichimaru, K. Takayama and H. Ido: Jpn. J. Med. Phys. **23** (2003) 123.
14) E. Sato, Y. Hayasi, R. Germer, E. Tanaka, H. Mori, T. Kawai, T. Ichimaru, K. Takayama and Hideaki Ido: Rev. Sci. Instrum. **74** (2003) 5236.
15) E. Sato, K. Sato and Y. Tamakawa: Ann. Rep. Iwate Med. Univ. Sch. Lib. Arts and Sci. **35** (2000) 13.

研　究　論　文

Monochromatic polycapillary imaging utilizing a computed radiography system

Michiaki Sagae[1)*], Eiichi Sato[1)], Yasuomi Hayasi[1)], Etsuro Tanaka[2)], Hidezo Mori[3)], Toshiaki Kawai[4)], Haruo Obara[5)], Toshio Ichimaru[6)], Kazuyoshi Takayama[7)], Hideaki Ido[8)]

[1)] *Department of Physics, Iwate Medical University*
[2)] *Department of Nutritional Science, Faculty of Applied Bio-science, Tokyo University of Agriculture*
[3)] *Department of Cardiac Physiology, National Cardiovascular Center Research Institute*
[4)] *Electron Tube Division #2, Hamamatsu Photonics Inc.*
[5)] *Department of Radiological Technology, College of Medical Science, Tohoku University*
[6)] *Department of Radiological Technology, School of Health Sciences, Hirosaki University*
[7)] *Shock Wave Research Center, Institute of Fluid Science, Tohoku University*
[8)] *Department of Applied Physics and Informatics, Faculty of Engineering, Tohoku Gakuin University*

Research Code No.: 200, 204.1
Key Words: monochromatic radiography, quasi-parallel radiography, x-ray lens, polycapillary plate

Abstract

A fundamental study on quasi-parallel radiography using a polycapillary plate and a copper-target x-ray tube is described. In the experiments, the tube voltage was regulated from 12 to 22 kV, and the tube current was regulated within 3.0 mA by the filament temperature. The exposure time was controlled in order to obtain optimum x-ray intensity, and the maximum focal spot dimensions were approximately 2.0 × 1.5 mm. The thickness and the inner capillary tube diameter of the polycapillary were 1.0 mm and 25 μm, respectively. Monochromatic x-rays were produced using a 10 μm-thick nickel filter with a tube voltage of 17 kV, and these rays were formed into quasi-parallel beams by the polycapillary. The radiogram was taken using a computed

* 岩手医科大学教養部物理学科〔〒020-0015 岩手県盛岡市本町通3-16-1〕: Department of Physics, Iwate Medical University
e-mail: msagae@iwate-med.ac.jp

radiography system utilizing imaging plates. In the measurement of image resolution, the spatial resolution hardly varied according to increases in the distance between the resolution-test chart and imaging plate using a polycapillary. A 50 μm tungsten wire could be observed, and fine blood vessels of approximately 100 μm were visible in angiography.

Received Jan. 7, 2004; revision accepted Jul. 5, 2004

1. Introduction

Monochromatic parallel radiography typically utilizes a synchrotron in conjunction with silicon single crystals and it has been applied in x-ray phase imaging[1-3]. It has also been applied in high contrast micro-angiography[4-7] because x-rays with energies of approximately 35 keV are absorbed effectively by the iodine-based contrast medium.

In order to produce monochromatic x-rays without using the synchrotron, we developed a molybdenum x-ray tube[8] with a transmission-type molybdenum target, which is used as a monochromatic filter for absorbing bremsstrahlung x-rays. In addition, from weakly ionized linear plasma, we found irradiations of intense and sharp characteristic x-rays[9-12].

Recently, several different x-ray lenses[13,14] have been developed, and a polycapillary plate[8-15] has been shown to be useful to perform quasi-parallel radiography with lower photon energy. For this, the plate thickness is about 1 mm, and it is very difficult to design a thicker plate due to technical limitation for increasing the strait capillary length.

In biomedical radiography, because the image processing can be done easily with a Computed Radiography (CR) system[16,17] utilizing imaging plates, the CR system is useful for monochromatic parallel radiography, regardless of whether the image resolution falls as compared with an x-ray film; the spatial resolution is primarily determined by the minimum sampling pitch of 87.5 μm.

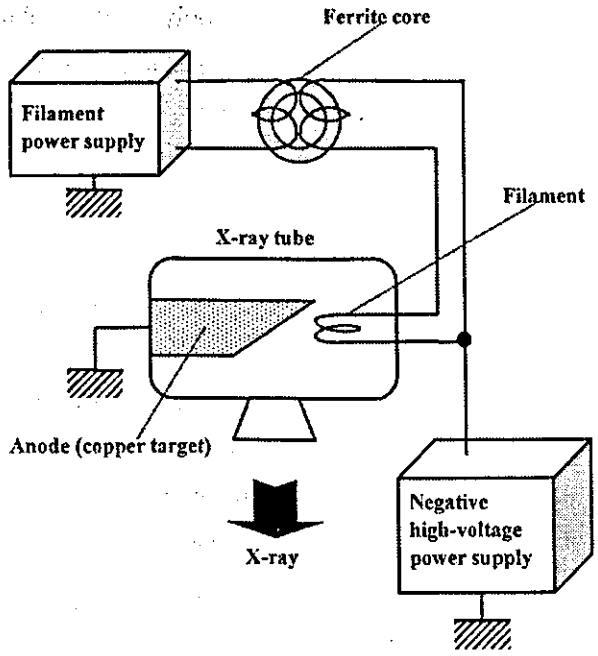

Fig. 1. Circuit diagram of the x-ray generator.

In this article, we describe a monochromatic quasi-parallel radiography system utilizing a polycapillary plate with an inner capilliary diameter of 25 μm, a CR system, and a copper-target radiation tube to realize a low-priced x-ray system utilizing an x-ray lens.

2. Experimental setup

Figure 1 shows the circuit diagram of the x-ray generator, which consists of a negative high-voltage power supply, a filament (hot cathode) power supply, and a copper-target x-ray tube. The negative high voltage is applied to the cathode electrode, and the anode (target) is connected to the ground. In the experiments, the

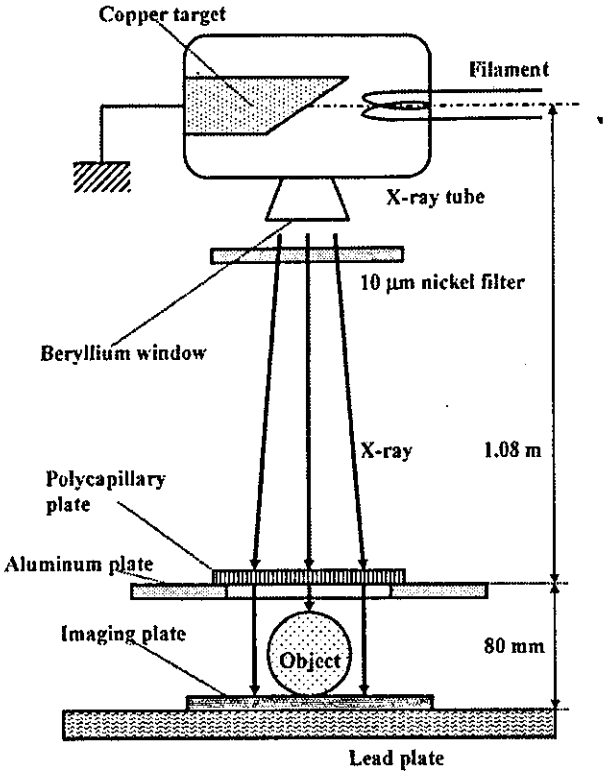

Fig. 2. Experimental setup for polycapillary imaging utilizing a CR system.

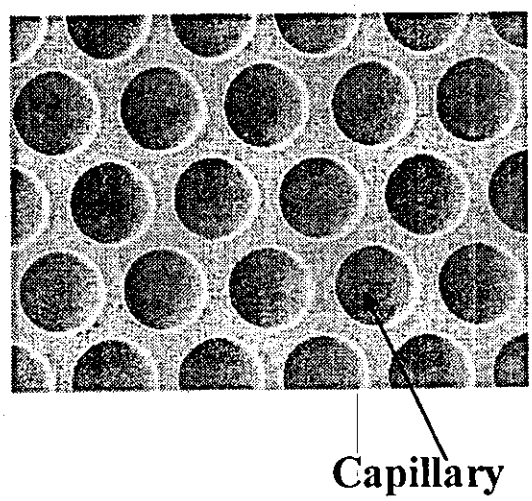

Fig. 3. Polycapillary plate.

tube voltage was regulated from 12 to 22 kV, and the tube current was regulated by the filament temperature and ranged from 1.0 to 3.0 mA. The exposure time was controlled in order to obtain optimum x-ray intensity.

The experimental setup for performing polycapillary imaging is shown in Fig. 2. Monochromatic x-rays were produced using a 10 μm-thick nickel filter, and these rays were formed into quasi-parallel beams by a polycapillary plate (Fig. 3). The polycapillary plate was J5022-21 (Hamamatsu Photonics Inc.), and the plate thickness was 1.0 mm. The outer, effective, and inner capilliary diameters were 87 mm, 77 mm, and 25 μm, respectively. Radiography was performed by a CR system (Konica Regius 150) utilizing imaging plates. The distance between the x-ray source and the polycapillary was 1.08 m, and the polycapillary plate was set on an aluminum plate. The distance between the polycapillary and imaging plates was regulated by the height (30 mm) of the polymethyl methacrylate (PMMA) spacers used.

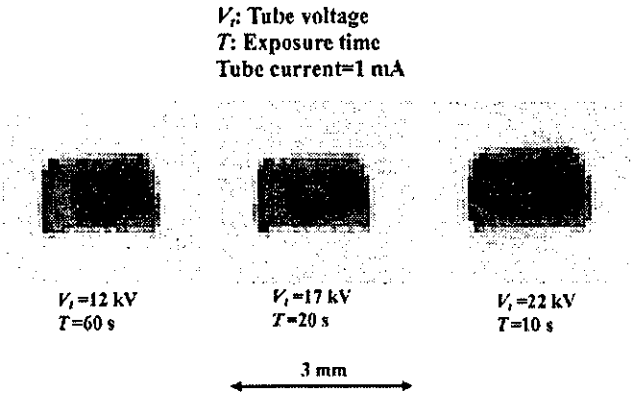

Fig. 4. Images of the x-ray source measured using a 50 μm-diameter pinhole while changing the tube voltage.

3. Characteristics

3.1. Focal spot

In order to measure images of the x-ray source, we employed the CR system, a pinhole camera with a hole diameter of 50 μm, and a filter (Fig. 4). When the tube voltage was increased, the focal spot intensity increased; spot dimensions also increased slightly and were approximately 2.0 × 1.5 mm.

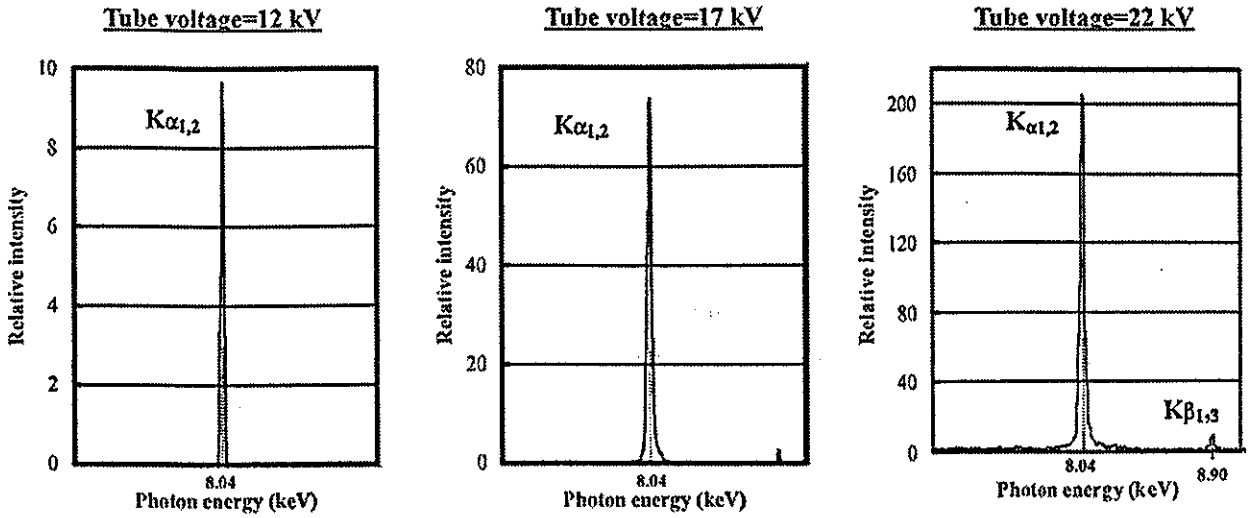

Fig. 5. Measured x-ray spectra while changing the tube voltage.

3.2. *X-ray spectra*

Monochromatic x-ray spectra from the copper-target tube were measured by a transmission-type spectrometer with a lithium fluoride curved crystal 0.5 mm in thickness. The spectra were taken by the CR system with a wide dynamic range, and relative x-ray intensity was calculated from Dicom digital data. Fig. 5 shows measured spectra from the copper target. When the tube voltage was increased, the characteristic x-ray intensity of Kα lines increased.

4. Radiography

The monochromatic radiography was performed with a tube voltage of 17 kV using the filter. Figure 6 shows radiography for imaging a polycapillary plate, and radiograms of the polycapillary are shown in Fig. 7. The center of the black spot in the polycapillary radiogram was mainly imaged by direct transmission beams through capillary holes. As shown in this figure, the spot dimensions increased slightly according to decreases in the PMMA spacer height.

Radiography for imaging a test chart for determining image resolution, and the radio-

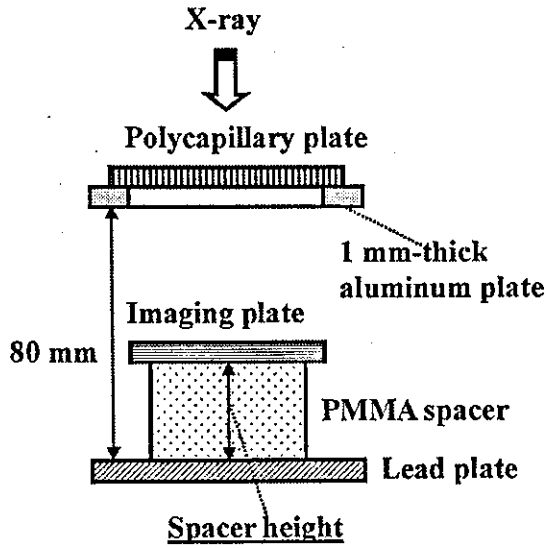

Fig. 6. Radiography for imaging a polycapillary plate while changing the distance between the polycapillary and imaging plates using PMMA spacers.

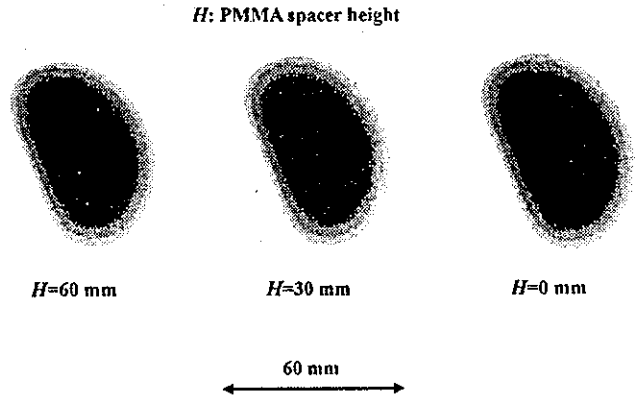

Fig. 7. Radiograms of a polycapillary plate while changing the PMMA height.

grams of 166 μm width lead lines, are shown in Figs. 8 and 9, respectively. Both the image resolution and the line contrast fell with decreases in the spacer height. Figure 10 shows the polycapillary radiography for imaging the test chart; the polycapillary was set on the aluminum plate. With this radiography system, we obtained higher contrast lines as compared with those in Fig. 9. When the spacer height was increased, the image resolution hardly varied, and the image dimensions decreased slightly (Fig. 11).

Figures 12 and 13 show radiography and the radiogram of tungsten wires on a PMMA box, respectively. Although the image contrast increased with increases in the wire diameter, a 50 μm-diameter wire could be observed. The angiography for a rabbit heart is shown in Fig 14; iodine-based microspheres of 15 μm diameter were used, and fine blood vessels of about 100 μm were visible (Fig. 15).

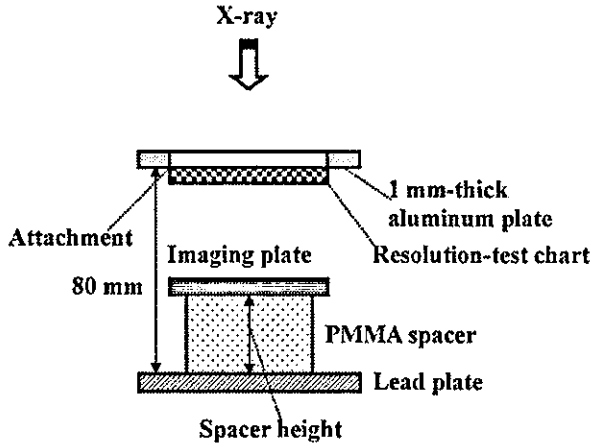

Fig. 8. Radiography for imaging a test chart according to the PMMA spacer height.

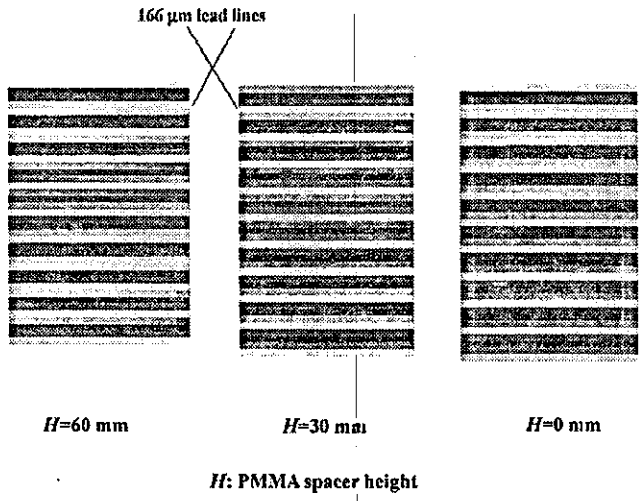

Fig. 9. Radiograms of a test chart according to the PMMA height.

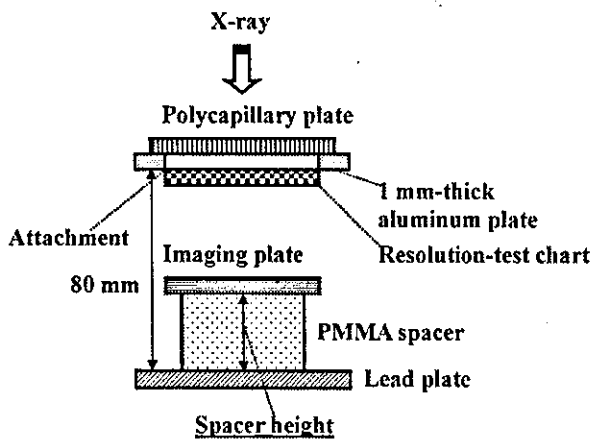

Fig. 10. Radiography for imaging a test chart using a polycapillary plate according to the PMMA height.

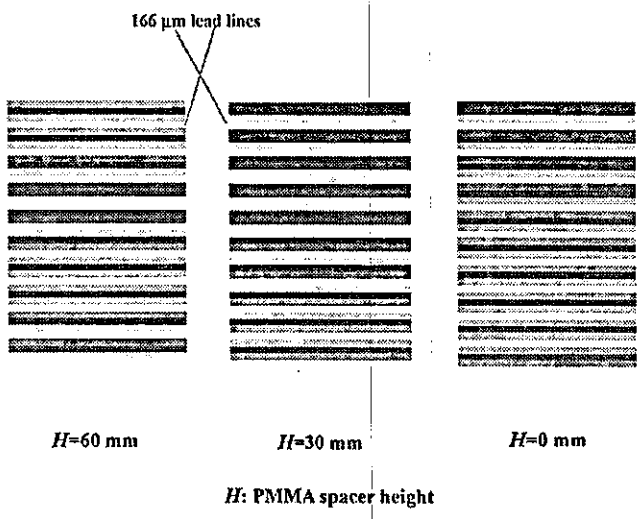

Fig. 11. Radiograms of a test chart using the polycapillary plate according to the PMMA height

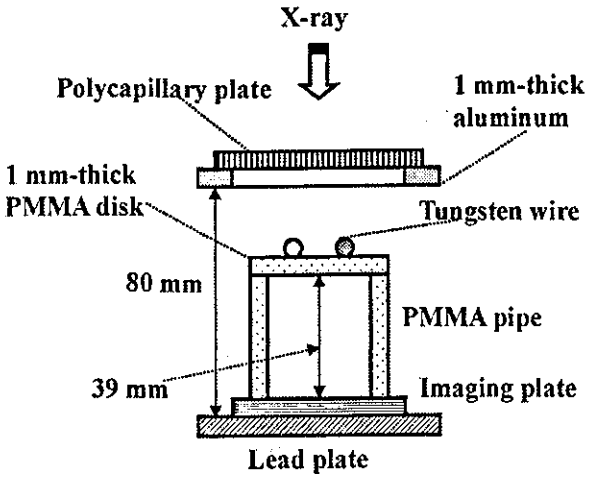

Fig. 12. Radiography for imaging tungsten wires using the polycapillary.

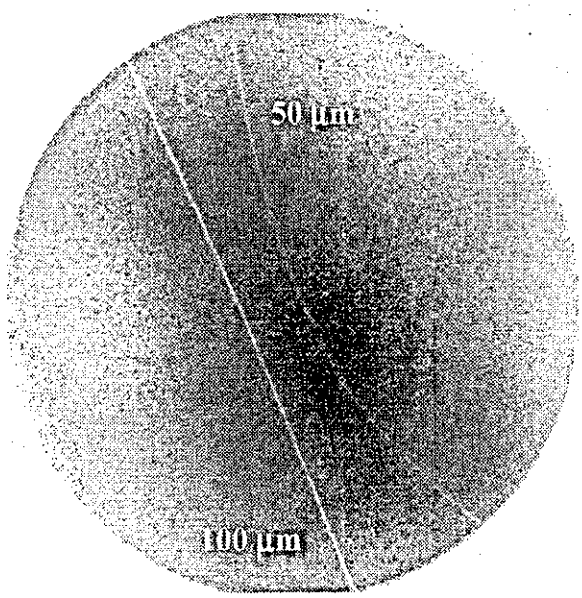

Fig. 13. Radiograms of tungsten wires on a PMMA spacer.

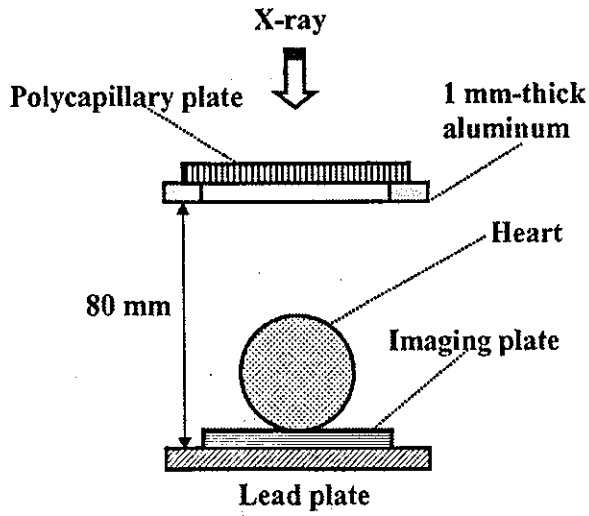

Fig. 14. Angiography using iodine-based microspheres of the heart extracted from a rabbit.

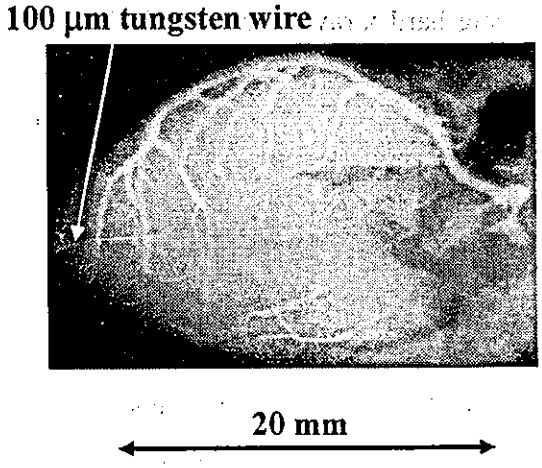

Fig. 15. Angiogram of the heart using the polycapillary.

5. Discussion

In this research, we carried out parallel radiography using a polycapillary plate in conjunction with monochromatic x-rays, and we obtained higher image resolutions as compared with those obtained without using the plate. Currently, the image resolution of the polycapillary is primarily determined by the inner capilliary diameter and the thickness, and it is improved with decreases in the diameter and increases in the thickness. In cases where the CR system is employed, although the resolution of the CR system is primarily determined by the minimum sampling pitch of 87.5 μm, we could observe 50 μm tungsten wires.

The photon energies of the characteristic x-rays are determined by the target element, and the capillary thickness should be increased according to increases in the photon energy because the transmission intensity through capillary glass increases. Subsequently, in order to increase the

parallelity for phase imaging, single crystals should be employed after passing the x-ray beam through the polycapillary.

Since it is possible to increase the irradiation field by increasing the distance between the x-ray source and the polycapillary, this system can be applied to image a wide variety of objects in various fields, including medical radiography.

Acknowledgments

This work was supported by Grants-in-Aid for Scientific Research (13470154, 13877114, and 16591222) and Advanced Medical Scientific Research from MECSST, Grants from Keiryo Research Foundation, The Promotion and Mutual Aid Corporation for Private Schools of Japan, JST (Test of Fostering Potential), NEDO, and MHLW (HLSRG, RAMT-nano-001, RHGTEFB-genome-005, and RGCD13C-1).

References

1) Davis T J, Gao D, Gureyev T E, et al.: Phase-contrast imaging of weakly absorbing materials using hard x-rays. Nature 373: 595-597, 1995
2) Momose A, Takeda T, Itai Y, et al.: Phase-contrast x-ray computed tomography for observing biological soft tissues. Nature Medicine 2: 473-475, 1996
3) Ishisaka A, Ohara H and Honda C: A new method of analyzing edge effect in phase contrast imaging with incoherent x-rays. Opt. Rev. 7: 566-572, 2000
4) Akisada A, Ando M, Hyodo K, Hasegawa S, et al.: An attempt at coronary angiography with a large size monochromatic SR beam. Nucl. Instrum. Meth. Phys. Res. A246: 713-718, 1986
5) Thompson A C, Zeman H D, Brown G S, et al.: First operation of the medical research facility at the NSLS for coronary angiography. Rev. Sci. Instrum. 63: 625-628, 1992
6) Mori H, Hyodo K, Tanaka E, et al.: Small-vessel radiography in situ with monochromatic synchrotron radiation. Radiology 201: 173-177, 1996
7) Hyodo K, Ando M, Oku Y, et al.: Development of a two-dimensional imaging system for clinical applications of intravenous coronary angiography using intense synchrotron radiation produced by a multipole wiggler. J. Synchrotron Rad. 5: 1123-1126, 1998
8) Sato E, Komatsu M, Hayasi Y, et al.: Quasi-monochromatic parallel radiography achieved with a plane-focus x-ray tube. SPIE 4786: 151-161, 2002
9) Sato E, Sagae M, Ichimaru T, et al.: Tentative study on x-ray enhancement by fluorescent emission of radiation by plasma x-ray source. SPIE 3771: 51-60, 1999
10) Sato E, Hayasi Y, Germer R, et al.: Intense characteristic x-ray irradiation from weakly ionized linear plasma and applications. Jpn. J. Med. Imag. Inform. Sci. 20: 148-155, 2003
11) Sato E, Hayasi Y, Germer R, et al.: Irradiation of intense characteristic x-rays from weakly ionized linear molybdenum plasma. Jpn. J. Med. Phys. 23: 123-131, 2003
12) Sato E, Hayasi Y, Germer R, et al.: Quasi-monochromatic flash x-ray generator utilizing weakly

ionized linear copper plasma. Rev. Sci. Instrum. 74: 5236-5240, 2003

13) Xiao Q F and Poturaef S V: Polycapillary-based x-ray optics. Nucl. Instr. Meth. Phys. Res. A 347: 376-383, 1994

14) MacDonald C A, Mail N, Li D, et al.: Monochromatic applications of polycapillary optics. SPIE 5196: 405-411, 2002

15) Sato E, Germer R, Hayasi Y, et al.: Quasi-monochromatic parallel flash radiography achieved with a plane-focus x-ray tube. SPIE 4948: 646-651, 2002

16) Sonoda M, Takano M, Miyahara J, et al.: Computed radiography utilizing scanning laser stimulated luminescence. Radiology 148: 833-838, 1983

17) Sato E, Sato K and Tamakawa Y: Film-less computed radiography system for high-speed imaging. Ann. Rep. Iwate Med. Univ. Sch. Lib. Arts and Sci. 35: 13-23, 2000

Optimal Windows of Statin Use for Immediate Infarct Limitation

5′-Nucleotidase as Another Downstream Molecule of Phosphatidylinositol 3-Kinase

Shoji Sanada, MD, PhD; Hiroshi Asanuma, MD, PhD; Tetsuo Minamino, MD, PhD; Koichi Node, MD, PhD; Seiji Takashima, MD, PhD; Hiroko Okuda, PhD; Yoshiro Shinozaki, MD, PhD; Akiko Ogai, PhD; Masashi Fujita, MD; Akio Hirata, MD; Jiyoong Kim, MD; Yoshihiro Asano, MD, PhD; Hidezo Mori, MD, PhD; Hitonobu Tomoike, MD, PhD; Soichiro Kitamura, MD, PhD; Masatsugu Hori, MD, PhD; Masafumi Kitakaze, MD, PhD

Background—Although statins are reported to have a cardioprotective effect, their immediate direct influence on ischemia-reperfusion injury and the underlying mechanisms remain obscure. We investigated these issues an in vivo canine model.

Methods and Results—Dogs were subjected to coronary occlusion (90 minutes) and reperfusion (6 hours) immediately after injection of pravastatin (0.2, 2, or 10 mg/kg), pitavastatin (0.01, 0.1, or 0.5 mg/kg), or cerivastatin (0.5, 5, or 50 μg/kg). Then myocardial phosphatidylinositol 3-kinase (PI3-K) and 5′-nucleotidase activities were measured, as well as infarct size. After 15 minutes of reperfusion, pravastatin caused dose-dependent activation of Akt and ecto-5′-nucleotidase in the ischemic zone, and the effect was significant at higher doses. Pitavastatin also significantly increased these activities, and its optimal dose was within the clinical range, whereas cerivastatin caused activation at the lowest dose tested. In all cases, both Akt and ecto-5′-nucleotidase showed activation in parallel, and this activation was completely abolished by wortmannin, a PI3-K inhibitor. The magnitude of the infarct-limiting effect paralleled the increase in Akt and ecto-5′-nucleotidase activity and was blunted by administration of wortmannin, α,β-methyleneadenosine-5′-diphosphate, or 8-sulfophenyltheophylline during reperfusion. Both collateral flow and the area at risk were comparable for all groups.

Conclusions—Activation of ecto-5′-nucleotidase after ischemia by PI3-K activation may be crucial for immediate infarct-size limitation by statins. There seems to be an optimal dose for each statin that is independent of its clinical cholesterol-lowering effect. **(*Circulation*. 2004;110:2143-2149.)**

Key Words: statins ■ myocardial infarction ■ adenosine ■ enzymes ■ phosphates

The 3-hydroxy-3-methylglutaryl coenzyme A reductase inhibitors (statins) block the biosynthesis of cholesterol[1] and are widely used clinically to decrease serum cholesterol levels. Recent studies have focused on the pleiotropic effects of either hydrophilic[2-4] or hydrophobic[4,5] statins, which are independent of their cholesterol-lowering effect.[2-4,5] Protection against ischemia-reperfusion injury is one of them, which is particularly evident after 12 hours.[6,7] In addition, some studies showed that statins activate the phosphatidylinositol 3-kinase (PI3-K)/Akt pathway within 1 hour,[8,9] as well as activating endothelial nitric oxide synthase (eNOS),[9,10] to cause immediate infarct limitation.[8]

On the other hand, other studies revealed that statins also acutely activate ecto-5′-nucleotidase,[11] which produces the endogenous cardioprotective substance adenosine,[12] especially in response to certain stresses.[13] Ecto-5′-nucleotidase can act only when localized on the cell membrane,[13] and the density of this enzyme on the membrane regulates its activity.[11,14] Endocytotic turnover of ecto-5′-nucleotidase (5′-nucleotidase localized on the cell surface) is inhibited by PI3-K activation,[14] which subsequently increases total 5′-nucleotidase activity within a period as short as 10 minutes.[14] Therefore, we hypothesized that an increase of ecto-5′-nucleotidase activity might be critical for early cardioprotec-

Received March 26, 2004; revision received May 4, 2004; accepted May 7, 2004

From the Department of Internal Medicine and Therapeutics (S.S., H.A., T.M., S.T., H.O., M.F., A.H., Y.A., M.H.), Osaka University Graduate School of Medicine, Suita; the Department of Cardiovascular and Renal Medicine (K.N.), Saga University Faculty of Medicine, Saga; the Department of Physiological Science (Y.S.), Tokai University School of Medicine, Isehara; and the Cardiovascular Division of Medicine (A.O., J.K., H.M., H.T., S.K., M.K.), National Cardiovascular Center, Suita, Japan

Correspondence to Masafumi Kitakaze, MD, PhD, Director, Cardiovascular Division of Medicine, National Cardiovascular Center, 5-7-1 Fujishirodai, Suita, 565-8565 Japan. E-mail kitakaze@zf6.so-net.ne.jp

Circulation is available at http://www.circulationaha.org

DOI: 10.1161/01.CIR.0000143830.59419.73

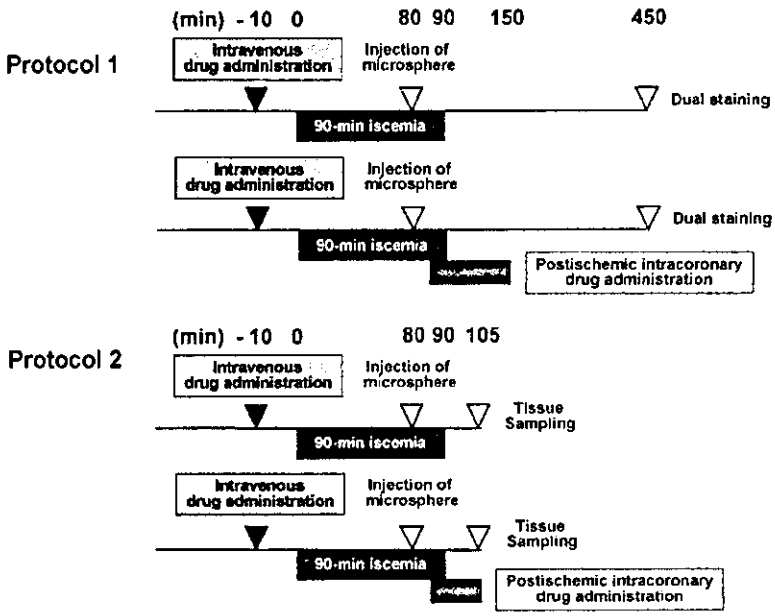

Figure 1. Experimental protocols to measure infarct size (protocol 1; Upper) and kinase activity (protocol 2; Lower).

tion mediated by statins and might be associated with rapid activation of PI3-K.

Here we used a dog model to determine whether 3 statins with different water solubilities (pravastatin, pitavastatin, and cerivastatin) could acutely limit infarct size, as well as whether adenosine and PI3-K were involved in the underlying mechanism.

Methods

All procedures were performed in conformity with the *Guide for the Care and Use of Laboratory Animals* (NIH publication No. 85-23, 1996 revision) and were approved by the Osaka University Committee for Laboratory Animal Use. Pravastatin, pitavastatin, and cerivastatin were obtained from Sankyo, Kowa, and Takeda Pharmaceuticals, respectively. The other drugs were obtained from Sigma.

Instrumentation

Beagle dogs weighing 8 to 13 kg were anesthetized and connected to an extracorporeal bypass tube as described previously.[15,16] In all experiments, the average baseline values of mean aortic blood pressure (ABP), heart rate (HR), and arterial blood Po_2 were 102±2.2 mm Hg, 129±2.5 min^{-1}, and 109±4.1 mm Hg, respectively. Both ABP and HR were measured continuously during the study.

Experimental Protocols

Protocol 1: Measurement of Infarct Size and Myocardial Collateral Blood Flow

After hemodynamic stabilization, we infused pravastatin (0.2, 2, or 10 mg/kg), pitavastatin (0.01, 0.1, or 0.5 mg/kg), cerivastatin (0.5, 5, or 50 μg/kg) or saline intravenously for 10 minutes before 90 minutes of sustained ischemia, which was followed by 6 hours of reperfusion (n=9 to 13 each). Some groups also received intracoronary administration of a selective ecto-5′-nucleotidase inhibitor (α,β-methyleneadenosine-5′-diphosphate [AMP-CP; 80 $\mu g \cdot kg^{-1} \cdot min^{-1}$]; a nonselective adenosine receptor antagonist (8-sulfophenyltheophylline [8-SPT; 50 $\mu g \cdot kg^{-1} \cdot min^{-1}$]); or a selective PI3-K inhibitor (wortmannin [1.5 $\mu g \cdot kg^{-1} \cdot min^{-1}$]) between 5 minutes before and 60 minutes after reperfusion. We measured infarct size and regional myocardial collateral blood flow during 90 minutes of ischemia as described previously.[15]

We have already confirmed in the same model that the doses of AMP-CP,[17] 8-SPT,[17,18] or wortmannin[19] used in this study were appropriate to block ecto-5′-nucleotidase, the adenosine receptors, or PI3-K, respectively. Figure 1 shows the details of this protocol, and the Table lists all of the groups studied.

Protocol 2: Myocardial Enzyme Assays

Another 54 dogs underwent a procedure identical to that of some groups from protocol 1 and were studied for enzyme assays (n=3 or 4 each). In this protocol, not only wortmannin (1.5 $\mu g \cdot kg^{-1} \cdot min^{-1}$) but also LY294002 (60 $\mu g \cdot kg^{-1} \cdot min^{-1}$) was used as another selective PI3-K inhibitor. After 15 minutes of reperfusion, a myocardial tissue sample was obtained from the ischemic border zone to ensure evaluation of viable ischemic myocardium and was used for the measurement of PI3-K and ecto-/endo-5′-nucleotidase activity. The myocardial tissue was rapidly frozen in LN_2 and stored at −80°C. Measurement of PI3-K and 5′-nucleotidase activity was done as reported previously[15,19] with minor modifications.

Criteria for Exclusion

To ensure that all of the animals included in analysis were healthy and were exposed to a similar extent of ischemia, the exclusion criteria reported previously[16] for hemodynamics, excessive collateral flow, and lethal arrhythmia were adopted.

Statistical Analysis

Results were expressed as mean±SEM, and the number of animals or experiments is shown as n. Statistical analysis was performed by ANOVA with a modified Bonferroni post hoc test, and significance was defined at $P<0.05$.

Results

Mortality and Exclusions in Protocol 1

Among 222 dogs used in protocols 1, 56 dogs met the exclusion criteria of ventricular fibrillation or excessive myocardial collateral blood flow (>15 $mL \cdot 100\ g^{-1} \cdot min^{-1}$). Therefore, 166 dogs completed these protocols satisfactorily and were included in the data analysis (Table).

Changes in Hemodynamic Parameters, Risk Area, and Collateral Blood Flow in Protocol 1

The changes in ABP and HR were comparable among all groups throughout the protocol (data not shown), and both the

TABLE 1. Mortality, Exclusion, Area at Risk, and Collateral Flow in Each Group in Protocol 1

Groups	Initial No	Excluded: Lethal Arrhythmia: During Ischemia	Excluded: Lethal Arrhythmia: After Reperfusion	Excluded: Excessive Collateral Flow	Final No	Area at Risk, %	Collateral Flow, mL/100 g per minute
Control	13	1	2	1	9	40.1±2.1	8.2±1.0
Prava							
0.2	9	0	1	0	8	38.8±2.0	8.4±1.2
2.0	10	0	0	2	8	39.1±2.2	8.9±1.1
10	10	0	0	2	8	39.6±2.1	8.9±1.4
Pitava							
0.01	9	1	1	0	7	38.7±2.2	8.1±1.3
0.1	11	0	1	2	8	39.3±2.0	9.2±1.5
0.5	10	1	0	2	7	39.9±1.9	8.8±1.5
Ceriva							
0.5	11	0	1	2	8	39.2±1.9	8.5±1.3
5.0	10	1	1	1	7	38.9±2.1	8.7±1.4
50	11	0	1	3	7	39.0±2.0	9.1±1.5
AMP-CP							
+Prava 10	9	0	2	0	7	40.4±2.3	8.6±1.3
+Pitava 0.1	9	0	1	1	7	39.8±2.0	8.4±1.5
+Ceriva 0.5	9	1	1	0	7	40.4±2.3	9.0±1.4
8SPT							
+Prava 10	10	0	1	1	8	38.7±2.2	8.3±1.3
+Pitava 0.1	11	1	2	0	8	39.9±2.1	8.2±1.6
+Ceriva 0.5	11	0	2	1	8	38.4±2.6	8.5±1.5
WTMN							
+Prava 10	10	0	2	1	7	38.6±2.3	9.5±1.5
+Pitava 0.1	10	0	2	0	8	38.9±2.1	9.2±1.6
+Ceriva 0.5	10	0	1	1	8	39.8±2.8	8.8±1.4
AMP-CP	9	0	2	0	7	38.8±2.5	8.5±1.6
8SPT	11	0	3	0	8	39.6±2.5	8.2±1.5
WTMN	9	1	2	0	6	40.5±2.3	8.6±1.6

Data expressed as mean±SEM. Prava indicates pravastatin (mg/kg); Pitava, pitavastatin (mg/kg); Ceriva, cerivastatin (μg/kg); 8SPT, 8-sulfophenyltheophilline, and WTMN, wortmannin.

area at risk and collateral blood flow were also comparable (Table).

Infarct Size

Figure 2 shows infarct size in the groups of protocol 1. Pravastatin (0.2, 2, and 10 mg/kg) dose-dependently reduced the infarct size (29.5±3.5%, 22.5±4.0%, and 18.8±3.4%, respectively) compared with that in the control group (39.8±3.6%), and the difference was significant at 2 mg/kg or more. Pitavastatin (0.01, 0.1, and 0.5 mg/kg) also reduced infarct size (32.9±3.9%, 23.6±3.8%, and 31.4±3.9%, respectively), although the optimal dose was 0.1 mg/kg (the only dose that produced a significant difference). Although cerivastatin (0.5, 5, and 50 μg/kg) caused infarct limitation (26.2±3.2%, 32.1±5.3%, and 37.1±4.4%, respectively), it was significant at the lowest dose only, and the effect was weaker at higher doses. Furthermore, cotreatment with AMP-CP, 8-SPT, or wortmannin between 5 minutes before and 60 minutes after reperfusion abrogated the infarct-limiting effect of pravastatin (39.9±4.0%, 42.6±4.0%, or 38.6±3.6%, respectively), pitavastatin (40.4±3.1%, 39.4±3.6%, or 39.1±3.1%, respectively), and cerivastatin (41.1±3.7%, 42.1±3.9%, or 40.4±4.0%, respectively), although these drugs per se did not affect infarct size (42.7±4.5%, 40.3±3.5%, or 42.7±4.5%, respectively).

5′-Nucleotidase Activity at Reperfusion

Figure 3 shows the activity of ecto-/endo-5′-nucleotidase in protocol 2. Sustained ischemia for 90 minutes and 15 minutes of subsequent reperfusion did not significantly change the activity of ecto-5′-nucleotidase (41.0±5.7 versus 33.2±1.2 nmol · mg protein^{-1} · min^{-1} at baseline). Preischemic treat-

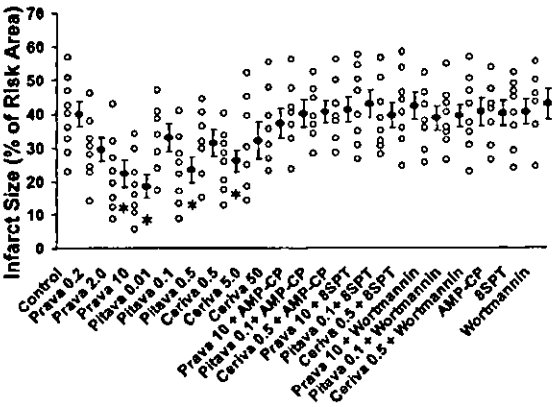

Figure 2. Infarct size in each group in protocol 1. Data are expressed as mean±SEM. *$P<0.05$ vs control. Open circles show infarct size in each individual. Prava indicates pravastatin; Pitava, pitavastatin; and Ceriva; cerivastatin. All other abbreviations are as defined in text.

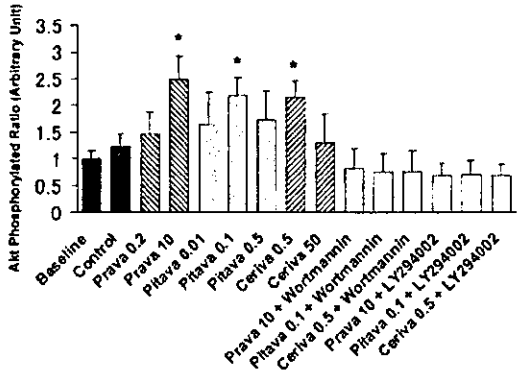

Figure 4. Myocardial PI3-K activity represented by phosphorylated ratio of Akt in each group in protocol 2. Data are expressed as mean±SEM. n=4 each, *$P<0.05$ vs control. Abbreviations are as defined in text and in legend to Figure 2.

ment with pravastatin caused a dose-dependent and acute increase of ecto-5′-nucleotidase activity in the ischemic zone, which became significant at the highest dose (72.6±6.0 nmol · mg protein^{-1} · min^{-1} at 10 mg/kg, $P<0.05$ versus control). Pitavastatin also caused significant activation at its optimal (medium) dose (66.7±6.1 nmol · mg protein^{-1} · min^{-1} at 0.1 mg/kg, $P<0.05$ versus control). Cerivastatin caused activation at the lowest dose (62.5±5.6 nmol · mg protein^{-1} · min^{-1} at 0.5 μg/kg, $P<0.05$ versus control). All of these increases were canceled by the selective PI3-K inhibitors wortmannin (39.5±6.8 nmol · mg protein^{-1} · min^{-1} for pravastatin, 37.0±7.1 nmol · mg protein^{-1} · min^{-1} for pitavastatin, and 38.4±6.5 nmol · mg protein^{-1} · min^{-1} for cerivastatin) or LY294002 (33.5±6.5 nmol · mg protein^{-1} · min^{-1} for pravastatin, 35.0±6.2 nmol · mg protein^{-1} · min^{-1} for pitavastatin, and 37.5±6.7 nmol · mg protein^{-1} · min^{-1} for cerivastatin). The activity of endo-5′-nucleotidase remained unchanged in all cases.

PI3-K Activity at Reperfusion

Figure 4 shows the activity of PI3-K in protocol 2. Sustained ischemia for 90 minutes and subsequent reperfusion for 15 minutes did not change PI3-K activity significantly (123±23% versus 100±14% at baseline). Preischemic treatment with pravastatin caused dose-dependent and acute activation of ecto-5′-nucleotidase in the ischemic zone, which was significant at the highest dose (249±44% at 10 mg/kg, $P<0.05$ versus control). Pitavastatin also caused significant activation at its medium dose (218±34% at 0.1 mg/kg, $P<0.05$ versus control), whereas cerivastatin caused activation at the lowest dose (214±31% at 0.5 μg/kg, $P<0.05$ versus control). We confirmed that all of these increases were also blocked by wortmannin (81±38% for pravastatin,

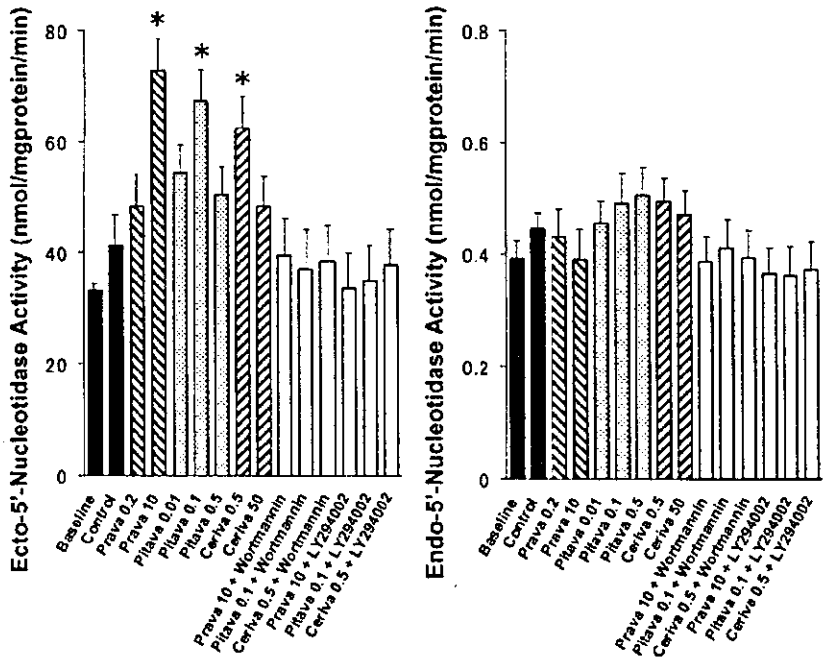

Figure 3. Myocardial ecto-/endo-5′-nucleotidase activity in each group in protocol 2. Data are expressed as mean±SEM. n=4 each, *$P<0.05$ vs control. Abbreviations are as defined in text and in legend to Figure 2.